Technical Physics, 2023, Vol. 68, No. 4

13

Composition and optical properties of amorphous plasma-chemical silicon oxynitride of variable composition $a-SiO_xN_y:H$

© V.A. Volodin,[1,2] G.N. Kamaev,[1] V.A. Gritsenko,[1,3] S.G. Chepkova,[1] I.P. Prosvirin[4]

[1] Rzhanov Institute of Semiconductor Physics, Siberian Branch, Russian Academy of Sciences, Novosibirsk, Russia
[2] Novosibirsk State University, Novosibirsk, Russia
[3] Novosibirsk State Technical University, Novosibirsk, Russia
[4] Boreskov Institute of Catalysis, Siberian Branch of RAS, Novosibirsk
E-mail: volodin@isp.nsc.ru

Received June 23, 2022
Revised January 16, 2023
Accepted February 2, 2023

The $a-SiO_xN_y:H$ films of various compositions were obtained by plasma chemical deposition from a gas mixture of 10% monosilane (diluted with argon) and nitrogen in the presence of residual oxygen in the working gas mixture. The nitrogen flow rate varied in the range from 4 to 6 cm^3/min, the power of the high-frequency generator (13.56 MHz) varied in the range of 50−150 Watts. The electronic structure and optical properties of the films were studied using X-ray photoelectron spectroscopy, vibrational spectroscopy, transmission and reflection spectroscopy, and spectral ellipsometry. It is shown that, as the generator power decreases, the content of excess silicon in the films increases and amorphous silicon nanoclusters appear. As the generator power increases, the oxygen concentration in the films decreases. Apparently, this is due to the greater dissociation of molecular nitrogen with an increase in the power of the plasma discharge and an increase in the concentration of active nitrogen. Thus, it is possible to control the composition of a$a-SiO_xN_y:H$ films not only by changing the nitrogen flow, but also by varying the generator power.

Keywords: silicon oxynitride, plasma-chemical deposition, stoichiometric composition, Si nanoclusters.

DOI: 10.21883/TP.2023.04.55947.167-22

Introduction

Dielectrics widely used in microelectronics, such as silicon oxide and silicon nitride, have recently all chances of being used in new elements of non-volatile memory, the memristors. For these purposes, films based on non-stoichiometric silicon oxide (SiO_x, $x < 2$) [1–4] and silicon nitride (SiN_x, $x < 4/3$) [5–7]. are most promising. Although SiO_x is currently closer to industrial use in ReRAM memristor arrays (WeeBit Nano announces industrial release of SiO_x-based ReRAM memory products as embedded arrays), it is still unclear whether silicon oxide or nitride will have better memory properties, and, accordingly, greater prospects. According to modern concepts, the transition of a memristor from a high-resistance state to a low-resistance state occurs during the passage of a pulse of current and the drift of oxygen vacancies in SiO_x or nitrogen in SiN_x with the formation of a conducting filament (a nanowire with a diameter of 1−5 nm enriched with silicon). It is known that the formation energy of an oxygen vacancy in SiO_x is less than the energy of formation of a nitrogen vacancy in SiN_x. So, it can be expected that the operation speed of memristors based on SiO_x in the mode of switching from a high-resistance state to a low-resistance state will be higher than the speed of memristors based on SiN_x. On the other hand, during the reverse process of switching from a low-resistance state to a high-resistance one, which occurs due to the diffusion of vacancies (oxygen in SiO_x and nitrogen in SiN_x) to a silicon filament, it can be expected that the process of filament annihilation in case of SiN_x will be slower compared to SiO_x. The time of information storage in a memristor is determined by the time of oxidation (in SiO_x) or nitriding (in SiN_x) of the silicon filament. Therefore, it can be expected that the information storage time in a memristor based on SiN_x will be longer than the time of information storage in a memristor based on SiO_x. Memristors based on SiO_x and SiN_x have both advantages and disadvantages It is quite possible that silicon oxynitride SiO_xN_y, consisting of Si−O and Si−N bonds, and in the case of silicon enrichment, also of Si−Si bonds [8,9], will combine the virtues of both materials. Thus, the purpose of this work is to study the electronic structure and optical properties of amorphous hydrogenated silicon oxynitride of variable composition $a-SiO_xN_y:H$ obtained at low temperature. The use of processes with a low thermal budget is extremely important, as it allows obtaining memristor structures at the end of all technological processes (the so-called back-end-of-line processes [10]). Recently, the possibility of creating memristors based on films of hydrogenated silicon oxynitride ($a-SiO_xN_y:H$) for neural networks [11] has been demonstrated.

1. Experimental procedures

Non-stoichiometric hydrogenated silicon oxynitrides ($a-SiO_xN_y:H$) were obtained by plasma-assisted (plasmo-

chemical) deposition from the SiH_4-N_2 gas mixture under controlled gas flow. Homogeneous $a-SiO_xN_y:H$ films were deposited on KDB-7.5 Si (100) p wafers cleaned of natural oxide on a plasmochemical deposition setup with a wide-aperture source and inductive excitation (the excitation frequency being 13.56 MHz). The residual pressure in the working chamber was less than 10^{-6} Torr and was achieved using a TMN-1500 turbomolecular pump, which also operated during film growth. The flow of monosilane supplied to the reaction zone (gas mixture of 10% SiH_4, diluted by Ar) was constant and amounted to 10 cm^3/min. The films of $a-SiO_xN_y:H$ with various compositions were obtained by varying the flow rate of N_2 in the range from 4 to 6 cm^3/min and the power of the high-frequency generator in the range of 50–150 W. Oxygen entered the reaction zone as a residual impurity to the working gases. The substrate temperature was maintained at 200°C.

The energy spectrum and stoichiometric composition of the $a-SiO_xN_y:H$ films were determined from the analysis of X-ray photoelectron spectroscopy (XPS). XPS data were obtained using a SPECS spectrometer equipped with an Al/Ag double anode X-ray source, a FOCUS-500 ellipsoidal crystal X-ray monochromator, a PHOIBOS 150 hemispherical electron analyzer, and an ion source. The spectra were obtained using Al K_α monochromatic radiation ($h\nu = 1486.74$ eV) with the analyzer transmission energy of 20 eV. The binding energy of the experimental peaks was calibrated using the peak C 1s at 284.8 eV associated with hydrocarbons on the surface of the samples. Spectral information was analyzed using XPSPeak 4.1 software [12]. The measurement techniques is described in more detail in [13].

Since the XPS method is surface-sensitive, an assessment was made of the depth of analysis of the studied samples. Using the QUASES-IMFP-TPP2M program [14], the free paths of photoelectrons for $a-Si$, Si_3N_4, and SiO_2 were estimated. Based on the obtained data, the depth of analysis of $a-SiO_xN_y:H$ films is a few nanometers [15].

The structural properties of $a-SiO_xN_y:H$ films were also studied using vibrational spectroscopy methods, both Raman scattering (RS) and Fourier transformed infrared (FTIR) spectroscopy. The Raman spectra were recorded using a T64000 spectrometer (Horiba Jobin Yvon) at room temperature in backscattering geometry; for excitation, an Ar^+ laser line with a wavelength of 514.5 nm was used. The spectral resolution was not worse than 2 cm^{-1}. The power of the laser beam reaching the sample was 1 mW, the beam spot diameter was 20 μm. Since the absorption of light with a wavelength of 514.5 nm in these films is small, the measurement mode used did not lead to local heating of the samples during the measurement process. The Fourier spectrometer FT-801 („SIMEKS", Novosibirsk, Russia) was used to record IR absorption spectra. The spectral range of the device is from 650 to 4000 cm^{-1}, the spectral resolution is 4 cm^{-1}. A silicon substrate without a film was used to obtain the reference signal.

The optical properties of $a-SiO_xN_y:H$ films in the visible region of the frequency spectrum, as well as in the near IR and ultraviolet (UV) ranges, were studied using transmission spectroscopy and spectral ellipsometry. To study the transmission spectra of the $a-SiO_xN_y:H$ films, special satellite samples were grown under absolutely the same growth conditions, but on transparent fused quartz substrates. An SF-56 spectrophotometer („LOMO-Spektr", St. Petersburg, Russia) was used. The spectral resolution was 2 nm, the measurement range was from 1100 to 190 nm (from 1.13 to 6.53 eV, respectively). For the ellipsometric analysis of $a-SiO_xN_y:H$ films on an opaque silicon substrate, we used the spectral ellipsometer „ELLIPS-1891-SAG" (Rzhanov Institute of Semiconductor Physics, Siberian Branch of Russian Academy of Sciences) [13,16]. The spectral dependences of the ellipsometric angles $\Psi(E)$ and $\Delta(E)$ were measured in the photon energy range 1.12–4.96 eV. The spectral resolution of the instrument was ~ 0.01 eV, the angle of incidence of the light beam was 70°, a four-zone measurement technique was used, followed by averaging over all four zones.

2. Results and discussion

Usually, a mixture of monosilane (SiH_4), ammonia (NH_3) and nitrous oxide (N_2O), or dichlorosilane (SiH_2Cl_2), ammonia and nitrous oxide are used to grow silicon oxynitride films. The process with the use of ammonia is easily controlled, since the dissociation energies of monosilane and ammonia are close and amount to 3.1 and 3.6 eV, respectively (the dissociation energy of nitrogen is 9.9 eV). In addition, ammonia can dissociate in multiple steps with low energy consumption. The use of molecular nitrogen (N_2) makes it possible to reduce the hydrogen content in films [14,17].

In our case, we used N_2 and a gas mixture of 10% SiH_4 diluted with Ar. However, even the purest gases are known to contain residual traces of oxygen and water. Oxygen has a very high reactivity when interacting with silicon. Even its insignificant content in the plasma gas leads to a high oxide growth rate. At the same time, in earlier experiments on the oxidation of the silicon surface in oxygen plasma, a significant role of inert gases (He, Ne, Ar) was revealed during their controlled admixture into the plasma-forming medium. So, the effect of a high oxidation rate in a plasma formed predominantly by helium at a relatively low oxygen concentration was discovered [15,18].

Experiments were carried out aimed at considering the optical luminosity of plasma components with a change in the relative content of nitrogen in it (helium was used as a carrier gas at a flow of 78 cm^3/min). Measurements of the optical emission spectra of the plasma were carried out using a „Kvarts-2000" spectrometer in the wavelength range of 500–800 nm with a spectral resolution no worse than 0.3 nm.

In the spectra, pronounced emission lines of nitrogen N^* (a group of lines in the region of 664–672 nm) and residual oxygen O^* (line at 777 nm) were observed. Figure 1 shows the intensities of these lines as a function of the

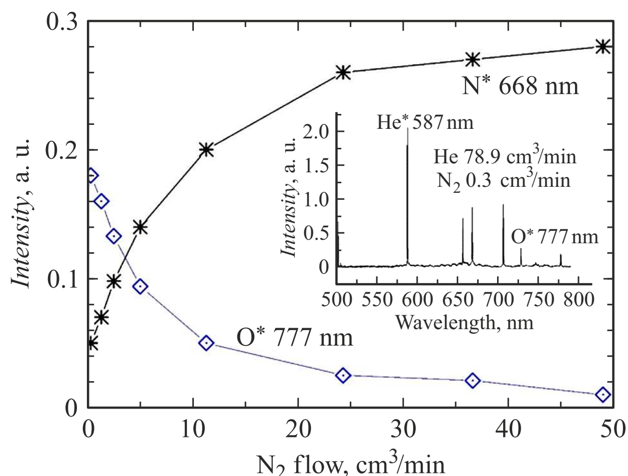

Figure 1. Dependence of the glow intensity of the plasma components on a change in the nitrogen flow. The inset shows the emission spectrum of the $He-N_2-O_2$ gas mixture plasma.

Table 1. Growth parameters of the studied a-SiO_xN_y:H films

Sample №	5-500	5-100	5-150	4-100	6-050	6-100
Flow of N_2, cm^3/min	5	5	5	4	6	6
Power of HF generator, W	50	100	150	100	50	100

flow of molecular nitrogen in standard cubic centimeters per minute. The inset to Fig. 1 shows the spectrum with luminescence lines. The power of the plasma discharge in this case was 450 W. It can be seen that with an increase in the nitrogen flow, the intensity of the emission line of atomic nitrogen N^* increases, which, in general, is obvious. But an interesting effect of suppressing the intensity of the atomic oxygen O^* line is also observed, although the concentration of residual oxygen does not change. This effect is observed when the proportion of a component with a significantly lower ionization energy increases in the plasma-forming mixture. In our case, it is nitrogen. Thus, an increase in the proportion of nitrogen should lead to a decrease in the proportion of active oxygen, and, accordingly, to a decrease in the concentration of Si–O bonds in the deposited $a-SiO_xN_y:H$ films.

Thus, a set of samples was grown at various nitrogen flows and at various plasma discharge powers. The parameters of the samples are shown in Table 1.

Figure 2 shows the photoelectron spectra of the Si2p level in silicon oxynitride of variable composition ($a-SiO_xN_y:H$) deposited in different regimes, as well as the spectra of amorphous silicon (a–Si), silicon nitride (Si_3N_4), and silicon oxide (SiO_2) for comparison. The vertical lines indicate the position of the Si2p level in silicon Si (99.4 eV), silicon nitride Si_3N_4 (101.7 eV), and silicon oxide SiO_2 (103.4 eV). The peak with an energy of 103.2 eV in silicon is due to a thin layer of natural oxide on its surface. It can be seen that samples 5-050, 5-100, 5-150, 6-100 are a mixture of silicon oxide, silicon nitride and silicon in different proportions.

This conclusion is confirmed both by the photoelectron spectra of the valence band and by the subvalent states of oxygen and nitrogen (Fig. 3). The peak with a binding energy of 25.3 eV corresponds to the O2s oxygen level in SiO_2 (it is especially visible in the spectrum of silicon dioxide). The broad peak with the binding energy $\sim$ 19 eV corresponds to the N2s nitrogen level in SiN_x. The obtained binding energies of these peaks are in good agreement with the literature data [19–22]. Thus, according to photoelectron spectroscopy data, $a-SiO_xN_y:H$ is a system of substitutional solid solution type consisting of $SiO_\nu N_\delta Si_\eta$ tetrahedrons, where $\nu + \delta + \eta = 4$. In this case, in accordance with the octahedral Mott rule, the silicon atom, as in silicon, is coordinated by four atoms (oxygen, nitrogen, and silicon), the oxygen atom, as in SiO_2, is coordinated by two silicon atoms, and the nitrogen atom, as in Si_3N_4 is coordinated by three silicon atoms [8,9]. The difference between the oxynitride studied in this work and the oxynitride studied in [8] is that the oxynitride studied in [8] consists of Si–O and Si–N bonds, and in the present work, in addition to Si–O and Si–N bonds, there are

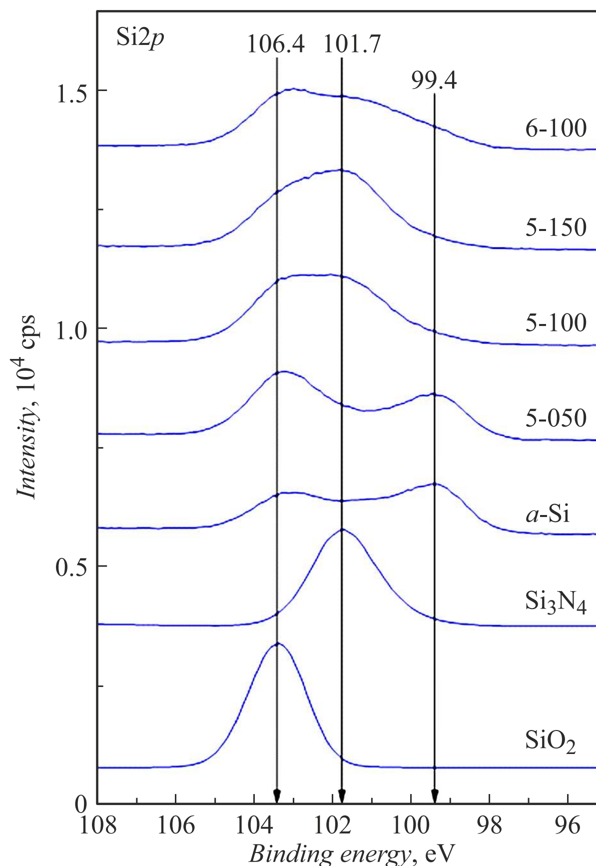

Figure 2. Photoelectron spectra of the Si2p level in silicon oxynitride $a-SiO_xN_y:H$ of variable composition, as well as in stoichiometric silicon dioxide and nitride.

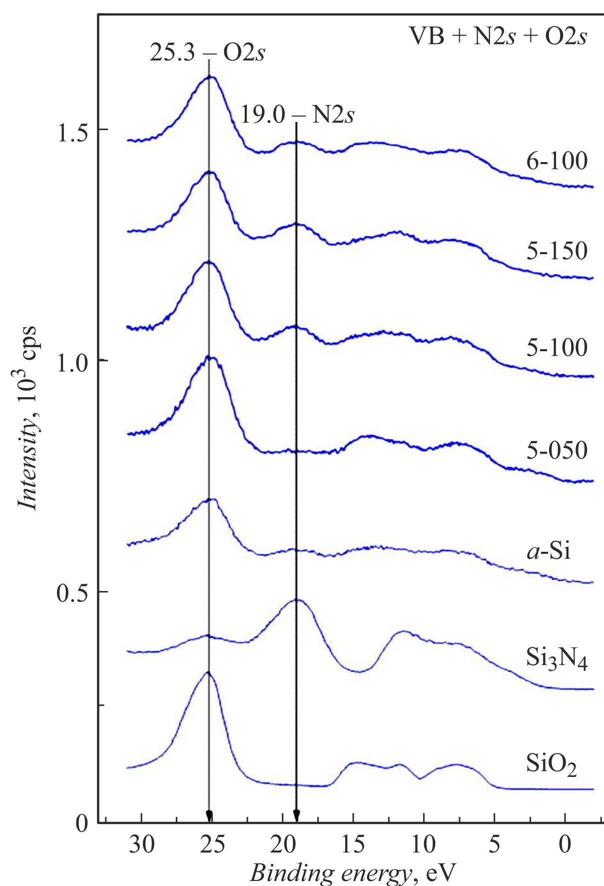

Figure 3. Photoelectron spectra of the valence band and subvalent levels O2*s* and N2*s* in silicon oxynitride $a-SiO_xN_y:H$ of variable composition, as well as in stoichiometric silicon dioxide and nitride.

also Si–Si bonds in the oxynitride. In other words, some oxynitride films studied in this work are enriched in excess silicon

Quantitative analysis of the XPS spectra showed that there is a clear correlation between the power introduced into the plasma and the relative content of oxygen and nitrogen in the oxynitride films: with increasing power, the nitrogen concentration increases, while the oxygen concentration decreases. Thus, it is possible to control the composition of the $a-SiO_xN_y:H$ films not only by changing the nitrogen flow, but also by varying the power of the RF generator.

The Raman spectra analysis also confirms the presence of excess silicon (Si–Si bonds) in some $a-SiO_xN_y:H$ films. Raman spectra were recorded for films grown on both silicon and quartz substrates, but Fig. 4 shows the spectra only for films grown on quartz substrates. This is due to the fact that the films are almost transparent, and their spectra exhibit intense lines from the silicon substrate, which complicates the analysis.

For comparison, Fig. 4 also shows the spectrum from a quartz substrate, and it can be seen that there are practically no features in the spectra of samples 5-150 and 6-100, except for the contribution from the substrate. It is known that local vibrations of Si–Si bonds in amorphous silicon give rise to features in the Raman spectra associated with the presence of maxima in the density of vibrational states. These are two broad-line modes with maxima at $\sim 480\,cm^{-1}$ (the contribution mainly from transverse optical modes — TO) and $\sim 150\,cm^{-1}$ (the contribution mainly from acoustic transverse modes — TA) [23]. The maximum contribution from these modes is observed in the spectra of the 5-050 and 6-050 films. In the spectra of samples 4-100 and 5-100, these modes are weak, but still visible against the background of the contribution from the substrate. So, we can conclude that, firstly, excess silicon begins to appear when the nitrogen flow decreases (comparison of samples 6-100, 5-100 and 4-100), which is natural, since the concentration of Si–N bonds decreases . Secondly, the amount of excess silicon increases with decreasing plasma discharge power (comparison of samples 5-150, 5-100 and 5-050). This is apparently due to the fact that the dissociation energy of monosilane is much lower than the dissociation energy of molecular nitrogen and oxygen.

The polar bonds Si–N, Si–O, Si–H, N–H, and others, which practically do not appear in the Raman spectra, appear in the IR absorption spectra shown in Fig. 5. All spectra are dominated by a peak at position $850-860\,cm^{-1}$, which corresponds to stretching modes of the Si–N bonds [24]. Also, in all spectra, stretching vibrations of

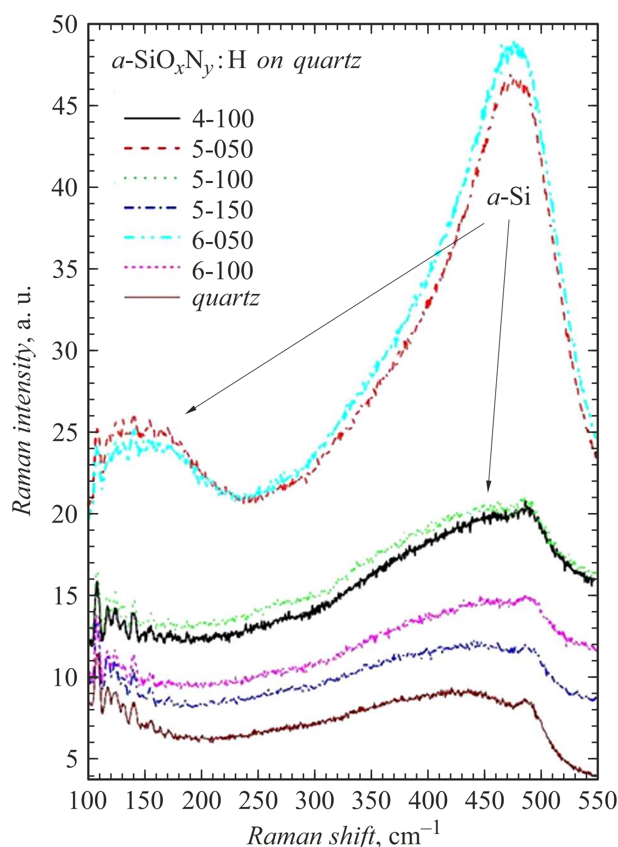

Figure 4. Raman spectra of $a-SiO_xN_y:H$ films; for comparison, the signal from the quartz substrate is also shown.

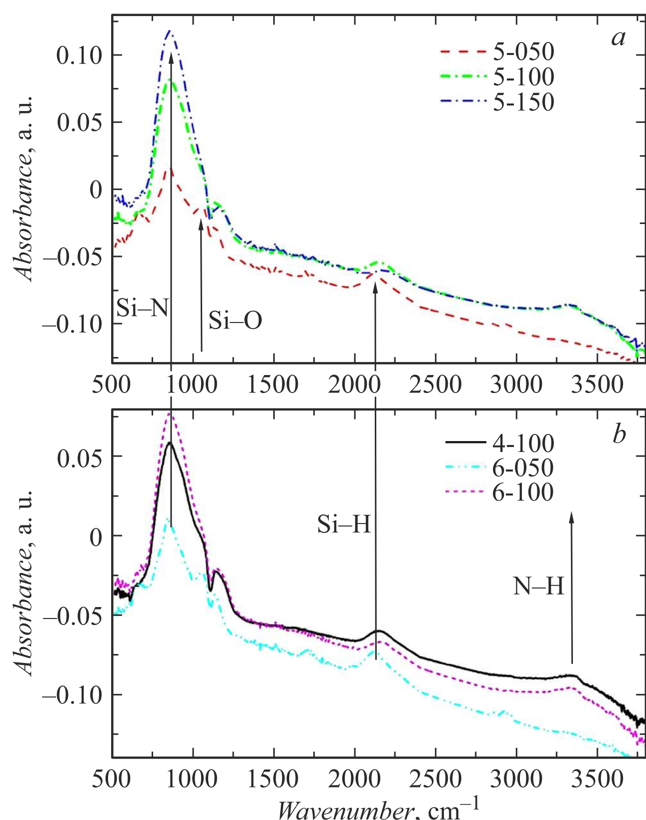

Figure 5. IR absorption spectra of $a-\mathrm{SiO}_x\mathrm{N}_y:\mathrm{H}$ films: a — samples with a nitrogen flow of 5 standard cubic centimeters per minute; b — samples with a nitrogen flow of 4 and 6 standard cubic centimeters per minute.

Si–O bonds appear in the form of singularities with the position $950-1050\,\mathrm{cm}^{-1}$. It is known that the frequency of this mode strongly depends on the nearest environment of silicon and oxygen atoms, in particular, on the stoichiometric parameter in SiO_x [24] films. As noted above, according to XPS data, silicon oxynitride films are a system of substitutional solid solution type consisting of $\mathrm{SiO}_\nu\mathrm{N}_\delta\mathrm{Si}_\eta$ tetrahedrons, where $\nu+\delta+\eta=4$. The frequency of local deformation vibrations of Si–O bonds is $\sim 1080\,\mathrm{cm}^{-1}$ at $\nu=4$ [18,25,26], and as the parameters δ and η increase, the frequency of these vibrations decreases [27] and in our case amounts to $\sim 950\,\mathrm{cm}^{-1}$. Thus, the IR spectroscopy data confirm the XPS data.

But unlike the XPS method, which cannot be used to analyze hydrogen bonds, the IR absorption method allows one to analyze these bonds. The dominant peaks associated with the presence of hydrogen in the films are the peaks due to stretching vibrations of Si–H bonds ($2080-2220\,\mathrm{cm}^{-1}$) and N–H bonds ($\sim 3335\,\mathrm{cm}^{-1}$). Whereas in the latter case the oscillation frequency is practically independent of the nearest environment of the nitrogen atom (the peak position is within $3325-3350\,\mathrm{cm}^{-1}$ [17,24,28]), in the case of Si–H bonds this dependence is essential. So, in the case of the $\mathrm{Si-Si_3H}$ tetrahedron, the frequency is $\sim 2000\,\mathrm{cm}^{-1}$, and in the case of the $\mathrm{Si-Si_2H_2}$ and $\mathrm{Si-SiH_3}$ tetrahedra, the frequency reaches $2100-2120\,\mathrm{cm}^{-1}$ [29]. In the case of $\mathrm{SiSi}_\nu\mathrm{N}_\delta\mathrm{H}_\eta$ tetrahedra, where $\nu+\delta+\eta=4$, the frequency will also depend on all three parameters ν, δ and η, and in our case, the position of the peak in different samples varies from 2080 to $2220\,\mathrm{cm}^{-1}$. Such a dependence was observed in $a-\mathrm{SiN}_x:\mathrm{H}$ films with a wide variation of the stoichiometric x [30].

It is also worth paying attention to the features associated with the presence of bending vibrations (bending modes) of various bonds. These are, first of all, the bonds Si–H [31] (a weak peak at $670\,\mathrm{cm}^{-1}$) and N–H [26] ($1150\,\mathrm{cm}^{-1}$). We should also note the presence of weak peaks at positions 1275 and $2970\,\mathrm{cm}^{-1}$, which can be associated with bending and stretching vibrations of C–H bonds, respectively [32]. This indicates that the films may contain carbon as a background impurity. Some spectra, after subtracting the background, were decomposed into component peaks (Gaussian curves) using the program Fityk [33] . The analysis of the peaks showed that, at the same nitrogen flow (Fig. 5, a), an increase in the plasma discharge power leads to a decrease in the amount of hydrogen in Si–H bonds and an increase in its content in N–H bonds. It is worth recalling here that nitrogen was used for growth, and monosilane was the source of hydrogen. Hydrogen, formed during the dissociation of monosilane, saturates the dangling bonds of nitrogen. The thickness of all films was approximately 200 nm, the method described in Refs. [12,24] was used to analyze the hydrogen concentration, the corresponding scattering cross sections were taken from [34–36]. Data on hydrogen concentration for films 5-050 and 5-150 are given in Table 2.

Figure 6 shows the transmission spectra of films deposited on transparent quartz substrates.

The transmission spectra of films grown on quartz substrates exhibited features associated with interference in the spectral region where absorption is weak. It is known that the absorption edge in stoichiometric silicon

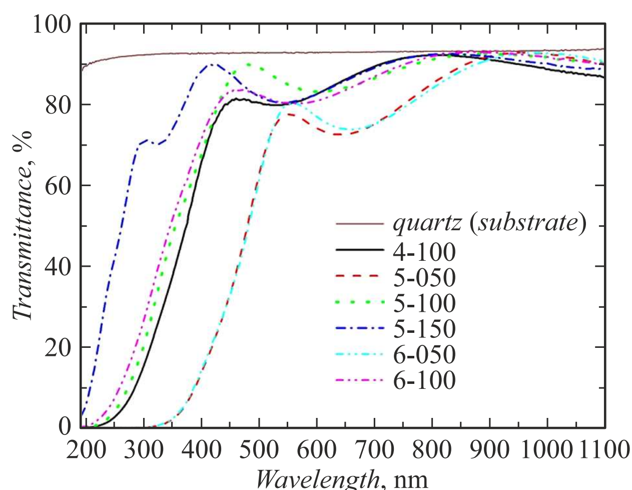

Figure 6. Transmission spectra of $a-\mathrm{SiO}_x\mathrm{N}_y:\mathrm{H}$ films in the visible range; for comparison, the transmission spectrum of the quartz substrate is also shown.

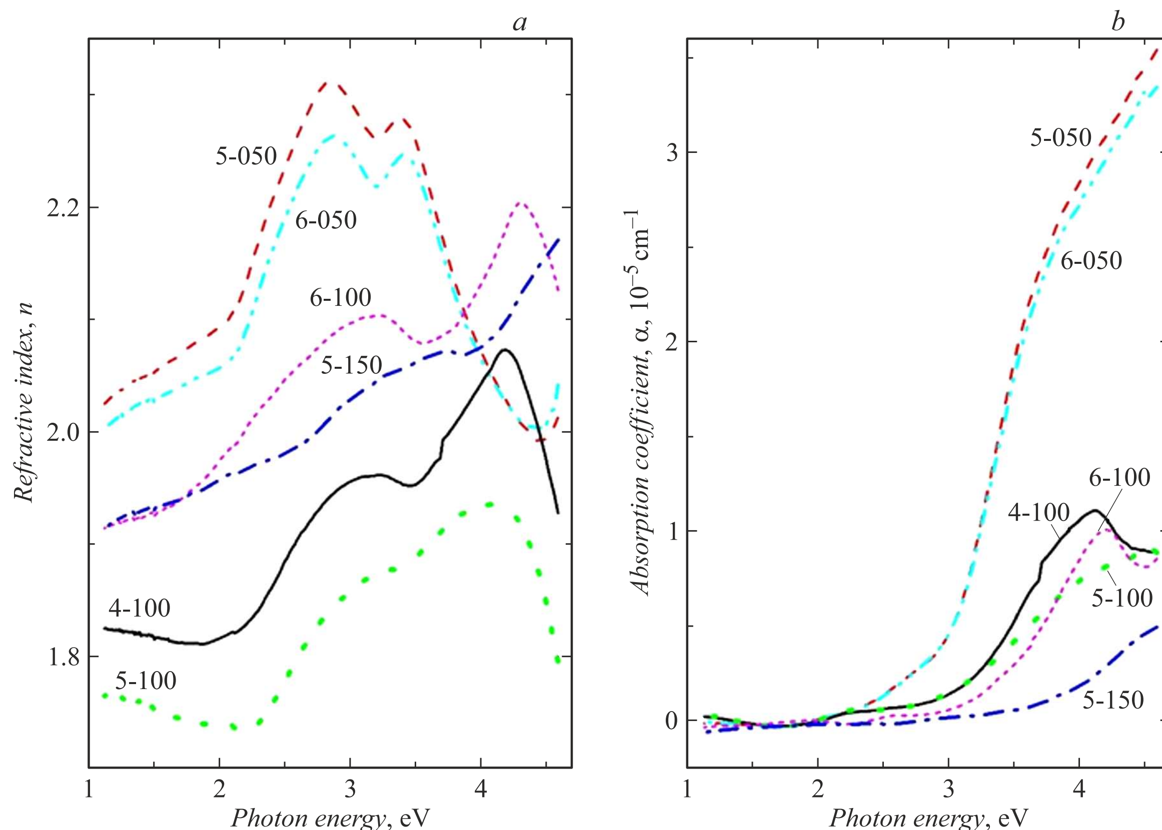

Figure 7. Dependences of the refractive index (n) and absorption coefficient (α) on the photon energy (E) for $a{-}\mathrm{SiO}_x\mathrm{N}_y$: H films .

Table 2. Hydrogen concentration in various chemical bonds in some $a{-}\mathrm{SiO}_x\mathrm{N}_y$: H films

Number of sample	Concentration of bonds N–H, 10^{22} cm^{-3}	Concentration of bonds Si–H, 10^{22} cm^{-3}
5-050	< 0.2	1.8
5-150	1.2	0.5

nitride is ~ 5 eV (~ 250 nm), while in amorphous silicon the absorption edge depends on the hydrogen content and varies from 1.5 to 2 eV [37]. In our case, due to the presence of interference, it was impossible to accurately determine the spectral dependence of the absorption coefficient and, accordingly, the absorption edge. Nevertheless, it can be seen in Fig. 6 that samples 5-050 and 6-050 with the largest excess of silicon are less transparent. And sample 5-150 is the most transparent, it contains practically no excess silicon. These data correlate with XPS, Raman spectroscopy, and IR absorption data.

The spectral ellipsometry data shown in Fig. 7 confirmed the transmission and reflection spectroscopy data. The inverse problem of ellipsometry (obtaining the optical constants of films from the analysis of ellipsometric angles) was solved as follows. In the single-film model, the spectral dependences of the ellipsometric angles $\Psi(E)_{calc}$ and $\Delta(E)_{calc}$ were calculated and fitted to the experimental dependences $\Psi(E)_{\exp}$ and $\Delta(E)_{\exp}$. The deviation of the calculated values from the experimental ones was minimized. The real part of the refractive index n of the films is shown in Fig. 7, *a*. Having known the imaginary part (k) of the refractive index, we can determine the absorption coefficient (shown in Fig. 7, *b*) as $\alpha = 4\pi k/\lambda$, where λ is the wavelength. In films of $a{-}\mathrm{SiO}_x\mathrm{N}_y$: H solid solutions, many factors affect the optical constants: excess silicon leads to an increase in the refractive index and absorption coefficient, and the presence of Si–O or Si–H bonds leads to a decrease in the refractive index and absorption coefficient. All this can be concluded from the analysis of spectral ellipsometry data. In samples 5-050 and 6-050 with the maximum content of excess silicon, the refractive index is maximum (Fig. 7, *a*), and the absorption edge (Fig. 7, *b*) is shifted to the low-energy range up to $\sim 2{-}2.5$ eV. As was noted above, the shift of the absorption edge in amorphous hydrogenated silicon can be due to the effect of hydrogen, but, in addition, the quantum-dimensional effect can also have an effect. It is known that as the size of silicon nanoclusters decreases, the absorption edge in them shifts to the short-wavelength region [38,39]. Unfortunately, it is impossible to separate these two effects, and only electron microscopy can provide information about the sizes of amorphous silicon nanoclusters in these films.

Both from the transmission spectra and from the spectral dependence of the absorption coefficient, it can be seen that the lowest absorption is observed for sample 5-150 with a minimum content of excess silicon. It should also be noted that in samples 4-100 and 5-100, the refractive index for the photon energy 2 eV is noticeably lower than the value 1.98 (the refractive index for stoichiometric silicon nitride). This is due to the fact that the concentration of Si–O bonds in these samples is maximum. For sample 5-150, the refractive index for photon energy 2 eV is 1.96, which is slightly less than the refractive index for stoichiometric silicon nitride; perhaps this is due to the presence of N–H and Si–H bonds.

Conclusions

It was demonstrated that during the growth of $a-SiO_xN_y:H$ films by means of plasma-chemical deposition from a mixture of SiH_4(10%)Ar(90%) and N_2 in the presence of residual oxygen in the working gas mixtures, their stoichiometric composition can be controlled not only by changing the nitrogen flow, but also by changing the power of the plasma discharge. With an increase in the generator power (frequency 13.56 MHz), the content of excess silicon decreases, and the oxygen concentration in the films also decreases. Apparently, this is due to the greater dissociation of molecular nitrogen with an increase in the power of the plasma discharge and an increase in the concentration of active nitrogen. Thus, the composition of the $a-SiO_xN_y:H$ films can be optimized to improve their memristor properties.

Acknowledgments

The authors are grateful to A.Kh. Antonenko for help in measuring the spectra of optical emission radiation. The authors are grateful to V.N. Kruchinin for help in measuring and interpreting the ellipsometry data. The authors are grateful to the Center for Collective Use „VTAN“ Novosibirsk State University, for providing the equipment for recording Raman spectra.

Funding

This study was financially supported by the Russian Science Foundation, project №22-19-00369.

Conflict of interest

The authors declare that they have no conflict of interest.

References

[1] A. Mehonic, A.L. Shluger, D. Gao, I. Valov, E. Miranda, D. Ielmini, A. Bricalli, E. Ambrosi, C. Li, J.J. Yang, Q. Xia, A.J. Kenyon. Adv. Mater., **30**, 1801187 (2018).

[2] M. Zackriya, H.M. Kittur, A. Chin. Scientific Reports, **7**, 42375 (2017).

[3] T. Kawauchi, S. Kano, M. Fujii. J. Appl. Phys., **124**, 085113 (2018).

[4] T.J. Yen, A. Gismatulin, V. Volodin, V. Gritsenko, A. Chin. Scientific Reports, **9**, 6144 (2019).

[5] T. Anutgan, M. Anutgan, I. Atilgan, B. Katircioglu. Appl. Phys. Lett., **111**, 053502 (2017).

[6] S. Kim, S. Jung, M.-H. Kim, Y.-Ch. Chen, Y.-F. Chang, K.-Ch. Ryoo, S. Cho, J.-H. Lee, B.-G. Park. Small, **14**, 1704062 (2018).

[7] T.J. Yen, A. Chin, V. Gritsenko. Scientific Reports, **10**, 2807 (2020)

[8] V.A. Gritsenko, J.B. Xu, I.H. Wilson, R.M. Kwok, Y.H. Ng, Phys. Rev. Lett., **81**, 1054 (1998).

[9] V.A. Gritsenko. UFN **178**, 727 (2008) (in Russian).

[10] J. Fan, O. Kapur, R. Huang, S.W. King, C.H. de Groot, L. Jiang. AIP Advances, **8**, 095215 (2018). https://doi.org/10.1063/1.5046564

[11] K. Leng, X. Zhu, Zh. Ma, X. Yu, J. Xu, L. Xu, W. Li, K. Chen. Nanomaterials, **12**, 311 (2022)

[12] Electronic source. Available at: http://xpspeak.software.informer.com/4.1/

[13] V.A. Gritsenko, V.N. Kruchinin, I.P. Prosvirin, Yu.N. Novikov, A. Chin, V.A. Volodin. ZhETF **156**, 1003 (2019). (in Russian).

[14] Electronic source. Available at: http://www.quases.com/products/quases-imfp-tpp2m/

[15] M.A. Isaacs, J. Davies-Jones, P.R. Davies, S. Guan, R. Lee, D.J. Morgan, R. Palgrave. Mater. Chem. Front., **5**, 7931 (2021). https://doi.org/10.1039/D1QM00969A

[16] V.N. Kruchinin, V.A. Volodin, T.V. Perevalov, A.K. Gerasimova, V.Sh. Aliev, V.A. Gritsenko. Opt. i spektr., **124**, 777 (2018) (in Russian).

[17] C. Doughty, D.C. Knick, J.B. Bailey, J.E. Spencer. J. Vacuum Sci. Technol. A, **17**, 2612 (1999).

[18] A.Kh. Antonenko, V.A. Volodin, M.D. Efremov, G.N. Kamaev, D.V. Marin, P.S. Zazulya. Avtometriya, **45**, 52 (2011) (in Russian).

[19] R. Reiche, F. Yubero, J.P. Espinos, A.R. Gonzalez-Elipe. Surf. Sci., **457**, 199 (2000).

[20] A.F. Zatsepin, D.A. Zatsepin, D.W. Boukhvalov, N.V. Gavrilov, V. Ya Shur, A.A. Esin. J. Alloys Compd., **728**, 759 (2017).

[21] V.A. Gritsenko, A.V. Shaposhnikov, W.M. Kwok, H. Wong, G.M. Jidomirov. Thin Solid Films, **437**, 135 (2003).

[22] P.M. Sylenko, A.M. Shlapak, S.S. Petrovska, O.Y. Khyzhun, Y.M. Solonin, V.V. Atuchin. Res. Chem. Intermed., **41**, 10037 (2015).

[23] J.E. Smith, Jr., M.H. Brodsky, B.I. Crowder, M.I. Nathan, A. Pinczuk. Phys. Rev. Lett., **26**, 642 (1971).

[24] G. Lucovsky, J. Yang, S.S. Chao, J.E. Tyler, W. Czubatyj. Phys. Rev. B, **28**, 3234 (1983).

[25] P.G. Pai, S.S. Chao, Y. Takagi, G. Lucovsky. J. Vacuum Sci. Technol. A, **4**, 689 (1986).

[26] C.T. Kirk. Phys. Rev. B, **38**, 1255 (1988).

[27] L.-N. He, T. Inokuma, S. Hasegawa. Jpn. J. Appl. Phys., **35**, 1503 (1996).

[28] T.T. Korchagina, D.V. Marin, V.A. Volodin, A.A. Popov, M. Vergnat. FTP, **43**, 1557 (2009) (in Russian).

[29] M.H. Brodsky, M. Cardona, J.J. Cuomo. Phys. Rev. B, **16**, 3556 (1977).

[30] H. Mäckel, R. Lüdemann. J. Appl. Phys., **92**, 2602 (2002).

[31] Yu.K. Undalov, E.I. Terukov, I.N. Trapeznikova. FTP, **53**, 1547 (2019) (in Russian).
[32] I.A. Averin, A.A. Karmanov, V.A. Moshnikov, I.A. Pronin, S.E. Igoshina, A.P. Sigaev, E.I. Terukov. FTT **57**, 2304 (2015) (in Russian).
[33] M.J. Wojdyr. J.Appl. Crystallography, **43**, 1126 (2010).
[34] A.V. Rzhanov (red.). *Nitrid kremniya v elektronike* (Nauka, SO, Novosibirsk, 1982) (in Russian).
[35] H.J. Stein, H.A.R. Wegener. J. Electrochem. Soc., **124**, 908 (1977).
[36] W.A. Lanford, M.J. Rand. J. Appl. Phys., **49**, 2473 (1978).
[37] G.D. Cody, B. Abeles, C.R. Wronski, R.B. Stephens, B. Brooks. Sol. Cells, **2**, 227 (1980).
[38] S. Furukawa, T. Miyasato. Phys. Rev. B, **38**, 5726 (1988).
[39] H. Rinnert, M. Vergnat, A. Burneau. J. Appl. Phys., **89**, 237 (2001).

Translated by Ego Translating